

## TROPICAL CYCLONES IN GFDL FVGFS

### – IMPACTS OF DYCORE, PHYSICS, AND INITIAL CONDITIONS

Jan-Huey Chen<sup>1\*</sup>, Xi Chen<sup>1</sup>, Shian-Jiann Lin<sup>1</sup>, Linus Magnusson<sup>2</sup>, Morris Bender<sup>1</sup>, Linjiong Zhou<sup>1</sup> and Shannon Rees<sup>1</sup>

<sup>1</sup>NOAA/GFDL, Princeton, NJ USA

<sup>2</sup>ECMWF, Reading, UK

#### 1. INTRODUCTION

A new global model using the GFDL (Geophysical Fluid Dynamics Laboratory) nonhydrostatic Finite-Volume Cubed-Sphere dynamical core (FV3) coupled to physical parameterizations from the National Center for Environmental Prediction's Global Forecast System (NCEP/GFS) was built at GFDL, named fvGFS. This modern dynamical core has been selected for National Oceanic and Atmospheric Administration's Next Generation Global Prediction System (NGGPS) due to its accuracy, adaptability, and computational efficiency, which brings a great opportunity for the unification of weather and climate prediction systems.

In this study, we investigated the performance of global TC forecasts in the early version of fvGFS based on 363 cases of 10-day forecasts in 2015. TC track and intensity forecast errors in the two fvGFS configurations were compared to those in the operational GFS. The results demonstrated the impacts of using different dynamical cores and cloud microphysics schemes in the model.

Preliminary results using different initial conditions in the fvGFS were also included in this study. Besides the pre-processing tool developed during the NGGPS Phase II to use the GFS analysis as the initial condition, a sophisticated interpolation tool was also developed in fvGFS to carefully use the ECMWF/IFS analysis data as the initial condition. The configuration of fvGFS and the interpolation method will be described in Section 2.

#### 2. MODEL, DATA AND METHODOLOGY

The fvGFS was built during the NGGPS Phase

II Dynamical Core Evaluation for testing the robustness of the dynamical core. The GFS physics package provided by NCEP/EMC (Environmental Modeling Center) was coupled to GFDL FV3. The hydrostatic version of FV3 (Lin, 2004) was extended to a non-hydrostatic solver. To achieve the non-hydrostatic approach, the hydrostatic pressure and geopotential were replaced with the non-hydrostatic full pressure and the true geopotential in the finite-volume pressure gradient scheme (Lin, 1997). The GFS physics package includes: Simplified Arakawa-Schubert (SAS) convection (Pan and Wu, 1995), Zhao-Carr grid-scale condensation and precipitation (Moorthi et al., 2001), the orographic and convective gravity wave drag of Kim and Arakawa (1995) and of Chun and Baik (1994), the boundary layer vertical diffusion of Hong and Pan (2011), and the Rapid Radiative Transfer Model (Clough et al., 2005).

To compare to the operational GFS with horizontal resolution about 13 km, the model configuration used in NGGPS phase II was C768 and 63 vertical levels with a model top at 0.64 hPa. The configuration of fvGFS for NGGPS phase II submission, called "FV3\_zc", did not include parameter tunings of any of the GFS physics. Therefore, the only major difference between FV3\_zc and the operational GFS forecast, called "GFS", is the dynamical core. The second configuration of fvGFS used the GFDL cloud microphysics scheme to replace the Zhao-Carr grid-scale condensation and precipitation scheme, but keeps other schemes in the GFS physics package unmodified, the configuration is called "FV3\_mp".

The GFDL simple tracker (Harris et al. 2016) was adopted for tracking TCs in the models. The errors of TC track and intensity and TC genesis performance were computed and evaluated based on Automated Tropical Cyclone Forecast best track

---

\* *Corresponding author address:*

Jan-Huey Chen, GFDL, 201 Forrestal Road,  
Princeton NJ 08536 USA;  
E-mail: Jan-Huey.Chen@noaa.gov

files which contain storm position and intensity information at 6-hourly intervals (Miller et al. 1990; Sampson and Schrader 2000).

The initial conditions for all 363 10-day forecasts were the GFS analysis data remapped from spectral space to the cubed-sphere geometry. The sea surface temperature were also provided by each date's GFS analysis but remained fixed from the initial time throughout the duration of each 10-day forecast. The fvGFS is also able to use the European Centre for Medium-Range Weather Forecasts (ECMWF) Integrated Forecasting System (IFS) data as the initial conditions.

During the initialization, geopotential height was first computed on the native data grid based on hydrostatic balance and ideal gas law. After that, all prognostic variables, including height, wind vector, and hydrometeors, were horizontally remapped from the latitude-longitude grid to any arbitrary point on the cubed-sphere grid (Putman and Lin 2007) based on the non-conservative bilinear interpolation in the  $(\lambda, \theta)$  space:

$$\eta^c = \gamma_{SW}\eta_{SW}^s + \gamma_{SE}\eta_{SE}^s + \gamma_{NW}\eta_{NW}^s + \gamma_{NE}\eta_{NE}^s \quad (1)$$

Where  $\eta$  is an arbitrary scalar to be regridded,  $\eta^s$  is the source values of  $\eta$  on the spherical grid,  $\eta^c$  denotes the value of  $\eta$  at the target location  $(\lambda^c, \theta^c)$ . The notations  $W, E, S, N$  stands for west, east, south, north and the location of  $\eta^c$  is within the rectangle formed by the four points of  $\eta_{SW}, \eta_{SE}, \eta_{NW}, \eta_{NE}$ . Denote the location of  $\eta^c$  is  $(\lambda^c, \theta^c)$ , and

$$\alpha = \frac{\lambda^c - \lambda_W}{\lambda_E - \lambda_W} \quad (2)$$

$$\beta = \frac{\theta^c - \theta_S}{\theta_N - \theta_S} \quad (3)$$

then

$$\gamma_{SW} = (1 - \alpha)(1 - \beta) \quad (4)$$

$$\gamma_{SE} = \alpha(1 - \beta) \quad (5)$$

$$\gamma_{NW} = (1 - \alpha)\beta \quad (6)$$

$$\gamma_{NE} = \alpha\beta \quad (7)$$

If the location of  $\eta^c$  is outside of the north or south bounds of the latitude-longitude grid the 2D bilinear interpolation is reduced to 1D linear interpolation:

$$\eta^c = (1 - \alpha)\eta_W^s + \alpha\eta_E^s \quad (8)$$

where  $\eta_W^s$  and  $\eta_E^s$  are at the north or south boundaries of the spherical grid. After the 2D horizontal remapping, a conservative track vertical polynomial-based interpolation was performed to regrid the prognostic variables into the model level for the dynamical core (Lin 2004; Chen et al. 2013).

### 3. RESULTS

#### 3.1 TC TRACK AND INTENSITY FORECASTS

Homogeneous comparisons of basin-wide mean TC track forecast errors along with the forecast lead-time are shown in Fig. 1. In the North Atlantic Ocean (Fig. 1a), the GFS and the two fvGFS configurations show similar track errors in the first 48 hours. However, both FV3\_zc and FV3\_mp show improved track forecasts compared to the GFS after the 60-hour lead-time. Similar results can be found in the North West Pacific basin, where the TC track forecast errors of the two fvGFS forecasts are smaller than those of GFS after 48-hour model lead-time (Fig. 1c). The track forecast errors of GFS and fvGFS are relatively close in the North East Pacific basin, where results indicate slightly lower errors for FV3\_mp after 84-hour lead-time than FV3\_zc and GFS (Fig. 1b).

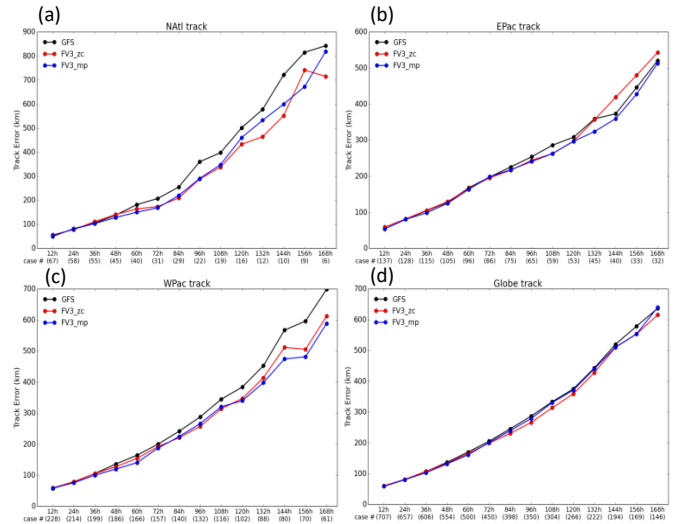


Figure 1. Mean TC track forecast errors (km) along with the model forecast lead time for GFS (black), FV3\_zc (red) and FV3\_mp (blue) in (a) the North Atlantic basin, (b) the North East Pacific basin, (c) the North West Pacific basin, (d) the globe.

The global mean TC track forecast errors are shown in Fig. 1d. The GFS shows slightly larger errors than the forecasts from the two fvGFS versions up to 168-hour lead time, while FV3\_mp

shows slightly larger TC track forecast errors than FV3\_zc for most lead times after 84h.

To investigate the performance of TC intensity forecasts, the wind-pressure relationships of TCs in GFS and FV3\_zc are compared to the best track data in Fig. 2. For intense cyclones with observed intensities exceeding  $40 \text{ ms}^{-1}$ , there is clearly a much better relationship between sea level pressure (SLP) and maximum 10-m wind speed for FV3\_zc than for the GFS. The model configuration of FV3\_zc uses a physics package nearly identical to that used in the GFS, while the horizontal resolutions of the two forecasts are also very close. Therefore, we believe that the differences shown in Fig. 2 are primarily from the replacement of the dynamical core. It is a very encouraging result that an advanced dynamical core is contributing to improving pressure-wind relationship for TCs in a global model.

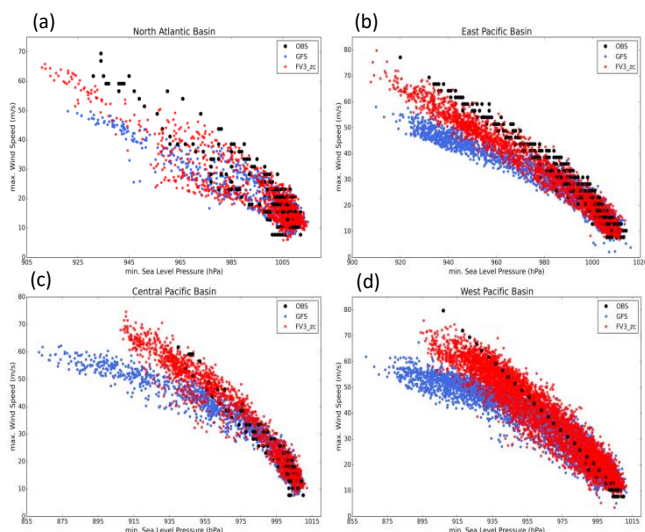


Figure 2. The relationship of maximum 10-m wind ( $\text{ms}^{-1}$ ) and minimum sea level pressure (hPa) for TCs in (a) the North Atlantic Ocean, (b) the North East Pacific basin, (c) the North Central Pacific basin and (d) the North West Pacific basin. Forecast data are plotted from every 6-hour lead time. The observations from ATCF best-track data are denoted in black dots. Forecasts of GFS cyclones are in blue dots and of FV3\_zc are in red.

Global mean forecast errors of intensity versus lead time are shown in Fig. 3. The biases of maximum 10-m wind speed shown in Fig. 3a indicate that the GFS under-predicted TC intensities until 132h, while FV3\_zc over-predicted intensities during the entire 7-day forecast. In contrast, the FV3\_mp shows very small negative intensity biases compared to FV3\_zc. Noted that at the 12-hour lead time, the GFS has a negative bias of  $4 \text{ ms}^{-1}$ , but there is almost no bias in either of the fvGFS forecasts which start from the same GFS initial

condition. It may indicate that fvGFS can better maintain the initial circulation than GFS. The differences of the maximum 10-m wind root-mean-square errors (RMSEs; solid lines in Fig.3a) among the three sets of forecasts are relatively small. Overall, during the first 84 hours, the two fvGFS versions show smaller RMSEs than those of the GFS, while the FV3\_mp is the best of the three. After 120-hour lead-time, GFS had lower errors than the fvGFS forecasts, but the RMSEs of FV3\_mp remained smaller than those of the FV3\_zc.

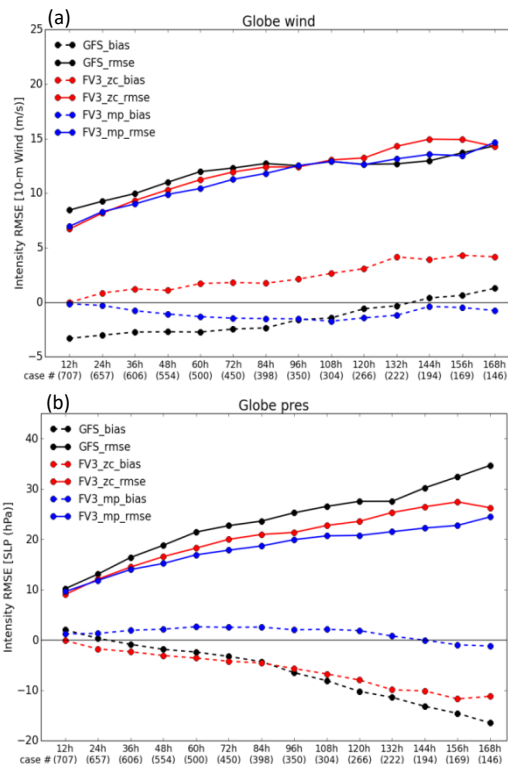


Figure 3. Global mean TC intensity forecast errors. (a) Maximum 10-m wind speed bias (dashed lines) and RMSE (solid lines,  $\text{ms}^{-1}$ ) along with the model forecast lead time for GFS (black), FV3\_zc (red) and FV3\_mp (blue). (b) As in (a), but for minimum sea level pressure (hPa).

The improvement of intensity forecasts in the FV3\_mp is also demonstrated by examining the bias and RMSE of the minimum SLP (Fig. 3b). Similar to the result for the maximum 10-m wind, the FV3\_mp only shows a slight bias during the 7-day forecasts, while both GFS and FV3\_zc show over-predicted intensity biases with an increasing trend toward deeper pressures with increasing lead time. The RMSEs of the three sets of forecasts are all increasing along with the lead time, while the FV3\_mp still shows the best intensity forecast performance of the three models.

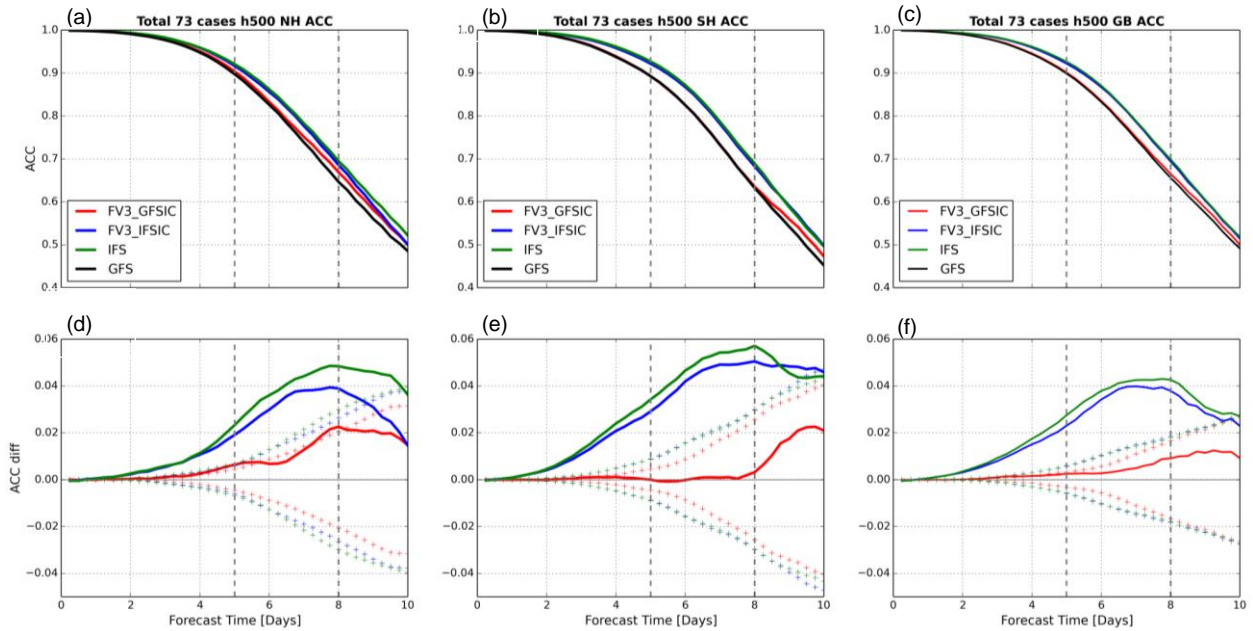


Figure 4. Mean 500-hPa height ACC for 73 10-day forecasts in (a) Northern Hemisphere, (b) Southern Hemisphere and (c) globe for GFS (black), FV3\_GFSIC (red), FV3\_IFSIC (blue) and IFS (green) verified against NCEP analysis data. Differences of 500-hPa height ACCs between FV3\_GFSIC and GFS (red), between FV3\_IFSIC and GFS (blue), and between IFS and GFS (green) in (d) northern Hemisphere, (e) southern Hemisphere and (f) globe. Dashed lines represent the 95% confidence intervals. Positive values indicate an improvement relative to the GFS.

### 3.2 TESTS USING DIFFERENT INITIAL CONDITIONS

The impact of using different initial conditions can be first examined in the global anomaly correlation coefficients (ACC) of 500-hPa height. Figures 4a-c show the ACCs for the fvGFS forecasts and GFS operational forecasts based on the GFS analysis data. The 73 cases of 10-day fvGFS forecasts were using GFS data (FV3\_GFSIC) and IFS data (FV3\_IFSIC) as the initial conditions. To highlight details of the ACC analysis, the ACCs of fvGFS, GFS and IFS forecasts are compared to the operational GFS forecasts in Figs. 4d-f. In the Northern Hemisphere, it can be found that the IFS model perform the best 10-day forecasts (Fig. 4a). The gap between GFS and IFS is about 0.05 on Day 8 (Fig. 4d). The ACC difference between FV3\_GFSIC and GFS on Day 8 is 0.02 which is regarded as the improvement from updating the dynamical core. When comparing FV3\_GFSIC and FV3\_IFSIC, it can be found that the improvement of ACC score from using the IFS initial condition is 0.02 as well. Note that simply interpolating the IFS data as the initial condition may not create a fully balanced initial field for the fvGFS. Also, the model resolution of fvGFS (13km) is lower than that of IFS (9km). Therefore, after adopting data assimilation and increasing model resolution, there should be a

chance for fvGFS to catch up with IFS's ACC performance in the future.

In the Southern Hemisphere, the improvement from using IFS initial conditions is even larger. The difference of ACCs between FV3\_IFSIC and IFS forecasts is less than 0.01 on Day 8 (Fig. 4e). At the same time, the ACC score of FV3\_IFSIC is 0.045 better than the FV3\_GFSIC.

TC track forecasts are associated with large-scale steering flow forecasts, which can be mostly represented by 500-hPa height ACC. Figure 5 shows the mean TC track forecast errors for GFS, FV3\_GFSIC and FV3\_IFSIC. In the North Pacific Ocean, including North West, North Central and North East Pacific basins, the FV3\_IFSIC shows smaller TC track errors than FV3\_GFSIC before 60-hour and after 144-hour lead-times (Fig.5a). There is a 15% improvement from using IFS initial condition at 48 hours, which is quite promising. In the Southern Ocean, the track forecast of FV3\_IFSIC is improved at 24, 36 and 72-hour lead-times, as well as after 132 hours. These preliminary results were based on the 73 forecasts which were initialized every 5 days to cover one year period. More forecast cases with higher temporal frequency will be needed to carry out a comprehensive analysis in the future.

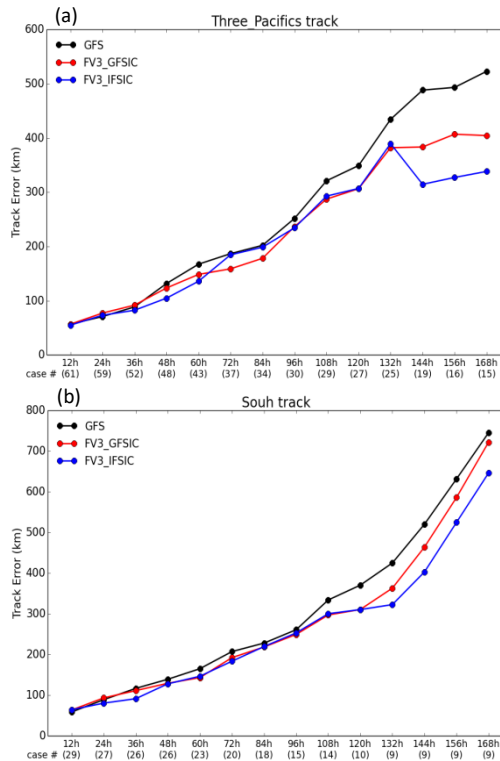


Figure 5. Mean TC track forecast errors (km) along with the model forecast lead time for GFS (black), FV3\_GFSIC (red) and FV3\_IFSIC (blue) in (a) the North Pacific Ocean and (b) the Southern Ocean.

#### 4. SUMMARY

The GFDL fvGFS (early version) shows better TC track and intensity forecasts than the operational GFS, especially in the northern Pacific Ocean. The impact to TC track forecasts by updating to the FV3 dynamical core in the GFS is positive, while there is a much improved wind-pressure relationship for FV3\_zc than for the GFS. The updated version with GFDL micro-physics shows a promising improvement in intensity prediction.

Forecasts of large-scale steering flow which affects TC movements can be mostly represented by the score of 500-hPa height ACC. Compared to the FV3\_GFSIC, FV3\_IFSIC shows large improvements on 500-hPa height ACCs in both Northern and Southern Hemispheres. The TC track forecasts in FV3\_IFSIC show smaller TC track errors in both northern Pacific Ocean and Southern Ocean as well.

#### References

Chen, X., N. Andronova, B. Van Leer, J. E. Penner, J. P. Boyd, C. Jablonowski, and S.-J. Lin., 2013:

A Control-Volume Model of the Compressible Euler Equations with a Vertical Lagrangian Coordinate. *Mon. Wea. Rev.*, **141**, 2526–2544.

Chun, H.-Y., and J.-J. Baik, 1994: Weakly Nonlinear Response of a Stably Stratified Atmosphere to Diabatic Forcing in a Uniform Flow, *J. Atmos. Sci.*, **51**(21), 3109-3121.

Clough, S. A., M. W. Shephard, E. Mlawer, J. S. Delamere, M. Iacono, K. Cady-Pereira, S. Boukabara, and P. D. Brown, 2005: Atmospheric radiative transfer modeling: a summary of the AER codes, *J. Quant. Spectrosc. Radiat. Transfer*, **91**(2), 233-244.

Harris, L. M., S.-J. Lin, and C. Tu, 2016: High-resolution climate simulations using GFDL HiRAM with a stretched global grid. *J. Clim.*, **29**, 4293–4314, doi:10.1175/JCLI-D-15-0389.1

Hong, S. Y., and H. L. Pan, 1996: Nonlocal boundary layer vertical diffusion in a Medium-Range Forecast Model, *Mon. Wea. Rev.*, **124**(10), 2322-2339.

Kim, Y.-J., and A. Arakawa, 1995: Improvement of Orographic Gravity Wave Parameterization Using a Mesoscale Gravity Wave Model, *J. Atmos. Sci.*, **52**(11), 1875-1902.

Lin, S.-J., 1997: A finite-volume integration method for computing pressure gradient force in general vertical coordinates, *Q. J. Roy. Meteorol. Soc.*, **123**(542), 1749-1762.

Lin, S.-J., 2004: A “vertically Lagrangian” finite-volume dynamical core for global models, *Mon. Wea. Rev.*, **132**, 2293-2307.

Miller, R. J., A. J. Scader, C. R. Sampson, and T. L. Tsui, 1990: The Automated Tropical Cyclone Forecast System (ATCF). *Wea. Forecasting*, **5**, 653–660.

Moorthi, S., H. L. Pan and P. Caplan, 2001: Changes to the 2001 NCEP operational MRF/AVN global analysis/forecast system, *NWS Technical Procedures Bulletin*, **484**, 14pp.

Pan, H. L., and W.-S. Wu, 1995: Implementing a mass flux convection parameterization package

for the nmc medium-range forecast model,  
*NMC Office Note*, **No. 409**, page 40pp.

Putman, W. M., and S.-J. Lin, 2007: Finite-volume transport on various cubed-sphere grids. *J. Comput. Phys.*, **227**, 55-78.

Sampson, C. R., and A. J. Schrader, 2000: The Automated Tropical Cyclone Forecasting System (version 3.2). *Bull. Amer. Meteor. Soc.*, **81**, 1231–1240.